Journal of Constructional Steel Research 183 (2021) 106762

Contents lists available at ScienceDirect

Journal of Constructional Steel Research

Hot-spot stress models of cutout detail on orthotropic steel bridge decks

Zhiwen Zhu [a,*], Jianpeng Li [b], Yan Huang [b], Alberto Carpinteri [a,c]

[a] Department of Civil and Environmental Engineering, Shantou University, Shantou, Guangdong 515063, China
[b] College of Civil Engineering, Hunan University, Changsha, Hunan 410082, China
[c] Department of Structural, Geotechnical and Building Engineering, Politecnico di Torino, Italy

ARTICLE INFO

Article history:
Received 23 December 2020
Received in revised form 12 May 2021
Accepted 15 May 2021
Available online 28 May 2021

Keywords:
Orthotropic steel deck
Fatigue
Cutout detail
Hot-spot stress
Field measurement
Random traffic flows

ABSTRACT

Stress distributions along the critical section of the floorbeam cutout detail of two different cutout geometries were studied based on bridge field tests. Stress concentration at cutout detail was significant and highly dependent on cutout geometry, hence nominal stress could not be applied. The existing HSS models failed to exclude significantly nonlinear stress at original cutout detail due to their first reference points too close to free edge of cutout, and hence they significantly underestimated fatigue life. A new HSS model, with two reference points located respectively 1.0 t and 1.5 t away from the free edge of cutout, was suggested and validated for the two types of cutout geometry. Because the retrofit cutout geometry increases stress at the area 0.5 t away from the free edge, the fatigue life using various HSS models is significantly low compared to the bridge design life. It is concluded that the suggested HSS model and FAT100 may be applicable to fatigue evaluation of cutout detail with different cutout geometry.

1. Introduction

The orthotropic steel decks (OSDs), one of the commonly used bridge deck system in steel bridge, are characterized by its favorite performance of light weight, low structure depth, rapid construction, high load carrying capacity and good durability. The OSDs are even popular in long-span bridges because dead loads reduction is a paramount concern to facilitate long-span crossing while to ensure structural safety. However, bridge engineering practice indicates that various cracks are frequently observed on fatigue-prone details on the OSDs [1], resulting from poor detailing, lack of control on welding process and the passage of extensively overweight trucks. Fatigue cracks on the OSDs may reduce the bridge structural integral, increase deck deflection, damage the deck overlay, degrade bridge ride quality, and even threaten bridge durability and structural safety.

Among the fatigue-prone details in the OSD, the floorbeam cutout detail has attracted more attention in recently years due to two great concerns link to cracks. One is that fatigue cracks were found on both early built and newly built bridges regardless years of praxis on such deck system; another is that some cracks at cutout detail can extend very long on the floorbeam web. Fatigue cracks at the floorbeam cutout have been observed on the Rio-Niteroi Bridge [2], the First Severn Crossing, the West Gate Bridge [3], and the Humen Bridge [4]. The Pingsheng Bridge, which is a self-anchored suspension bridge with main span of 350 m and was opened to traffics in the end of 2006, was reported with serious fatigue cracks in its OSDs, particularly at the floorbeam cutout detail [5]. When cracks at cutout detail were first observed by routine inspection staffs in 2013, some cracks were significantly long due to their lack of experience to find fatigue cracks at details of the OSDs. It suggests that this bridge has suffered from early cracking at the floorbeam cutout detail. Meanwhile, all cracked cutout details were directly underneath the design wheel track, indicating a strong correlation between the fatigue cracks and the traffic wheel loads.

In 2014, the OSDs in this bridge were then fully inspected to record crack location, length and direction. The inspection then found 121 cracks at the cutout detail, and they all initiated at the intersection point of the free edge of cutout with the critical section of the floorbeam web formed by floorbeam cutout (hereafter called "critical section" in short), and propagated upward at an incline angle around 15° to horizontal plane, as shown in Fig. 1. In the next years, to monitor if those cracks further propagate or new cracks appear at this detail, the steel box girder was inspected every two years. Fig. 1 shows the crack patterns and their development in the next years.

In recent years, the crack mechanism at the cutout detail and its countermeasure have received considerable attention through fatigue investigation. Generally, there are two types of method providing different stress to evaluate fatigue performance at this detail, i.e., the nominal stress method and the hot-spot stress (HSS) method. Connor [6] evaluated the effects of various cutout geometries on stress behaviors at fatigue-prone details based on FEM analysis. The nominal stress indicated that too shallow cutout geometries generated a strong constraint on the rib wall and in turns produced high stresses at the rib-to-floorbeam (RF) connection, while deep cutout geometries could

* Corresponding author.
E-mail address: zhuzw@stu.edu.cn (Z. Zhu).

https://doi.org/10.1016/j.jcsr.2021.106762
0143-974X/

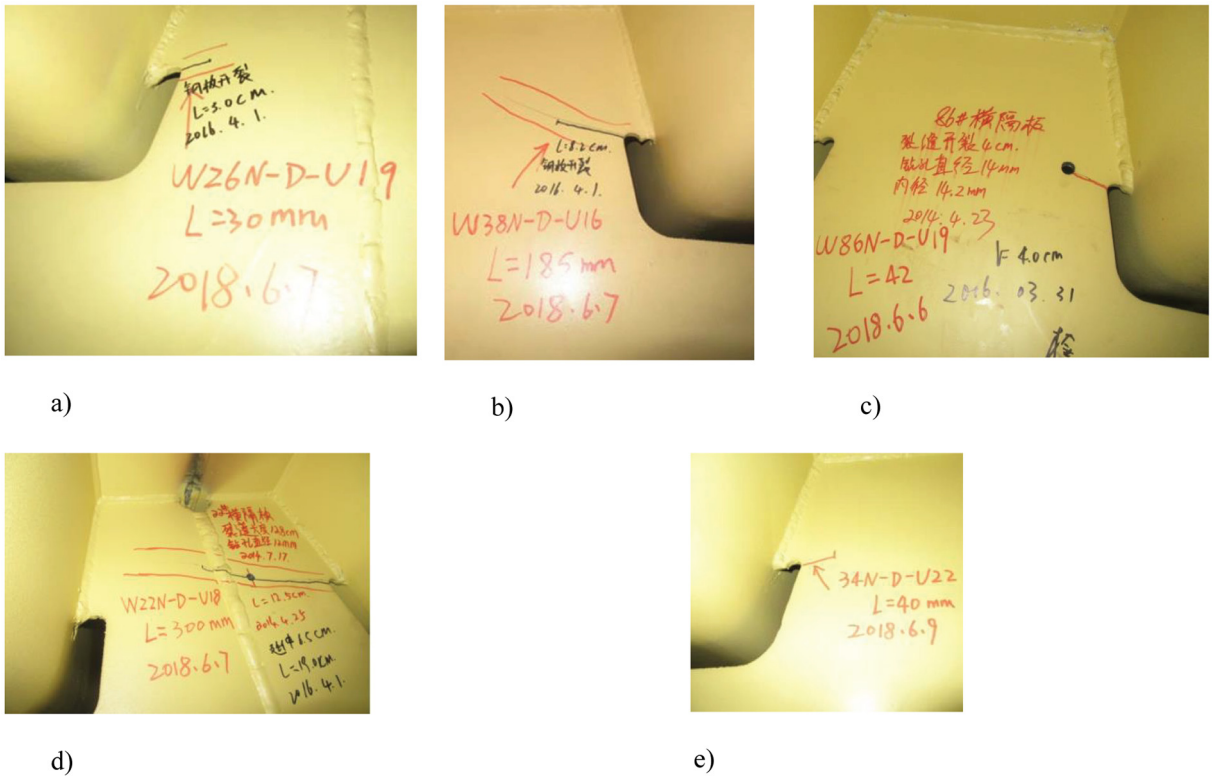

Fig. 1. Crack patterns and some development at cutout detail, a) no propagation; b) in propagation; c) arrested by stop hole; d) crack beyond stop hole; e) new crack found in 2018.

significantly weaken the floorbeam web and consequently increase the in-plane stress at the RF weld. Based on Vierendeel truss model and FEM analysis, Corte [7] carried out a parametric study on the effects of rib height and rib inclination on maximum stress at free edge of cutout, and cutout shapes were suggested for engineering application using the OSDs. Ye [8] investigated the stress behavior at the cutout detail based on FEM analysis, and concluded that the complex interaction between the deck plate, rib and diaphragm contributed to the high local stress at this detail. The study suggested the suitable height of RF weld, bottom location of bulkhead and cutout geometry, which aided in obtaining optimal stress at cutout detail. Based on field measurement under random traffic flow, Zhu [9] employed the nominal stress method to evaluate the fatigue life at the cutout detail of the OSD bridge using a steel-UHPC composite deck. Zhu [10] investigated the nominal stress at the cutout detail through multi-level finite element models. The research found that the cutout cracking was caused by a poor cutout geometry, thin diaphragms, a high truck traffic volume, and the overloaded wheel loads, as well as the lack of control on welding process. Deng [11] investigated the nominal stress at the cutout detail of a composite OSD under dynamic truck loads. The FEM results show that the composite OSD using the UHPC can effectively extend its fatigue life by at least 60% and even eliminate the risk of fatigue cracking at this detail.

The nominal stress method is only applicable to fatigue evaluation at a detail where the nominal stress is clearly defined. In other words, the nominal stress at the fatigue-prone detail will not be sensitive to the stress location. If the stress concentration appears with a high stress gradient, the nominal stress will be highly dependent on its location, which is the case for some fatigue-prone details in the OSDs, such as the floorbeam cutout detail, where different cutout geometries create the different level of stress concentration at the free edge of cutout. Consequently, the evaluated fatigue life may differ greatly with the stress obtained at different locations, and the nominal stress method may not be valid, as indicated in BS5400 that nominal stress should not be applied to the OSDs [12]. As regards the cutout detail in the OSDs, the FEM analyses also indicated a significant stress concentration at this location [13,14], which is truly dependent on the employed cutout geometry in the floorbeam web, more in detail, smaller the radius at the lower portion of the RF weld, more significant stress concentration at the cutout detail [8].

The HSS method is another frequently used approach in fatigue evaluation of engineering structures [15], and recently some studies have been conducted to investigate fatigue behaviors at various details in the OSDs. Cheng [16] carried out fatigue tests for full-scale rib-to-deck (RD) welded joints to investigate its fatigue cracking process and failure mechanics. They found that the HSS at the RD weld toe can be obtained by linear extrapolation, because the linear stress distribution is justified within the extrapolation region. Heng [17] introduced a stress concentration factor defined as the ratio of the HSS to the nominal stress. Based on the OSD model with the thickened edge U ribs, the fatigue tests found that the HSS on the deck plate side is only 1.2 times the nominal stress, although the nominal stress location is 1.5 times the thickness of the deck plate. They found that the use of thickened edge U ribs could enhance the fatigue strength of rib-to-deck joints.

Fu [18] studied the fatigue performance of RD welds with different penetration rates through fatigue tests and FEM analyses. They estimated the HHS based on the IIW two-reference-point scheme and three-reference-point scheme. The results revealed that an increased penetration rate can decrease the crack-propagation rate and enhance the fatigue life. Johan [19] established a linear-elastic fracture mechanics model to investigate the fatigue performance of the RD detail. They obtained the HSS at the root of the RD detail, and used it to predicted the fatigue life based on s crack growth rate. They predicted crack propagation modes at the different stage, and considered the effects of stiffness of road pavement on the HSS at the RD detail. Luo [20] carried out model tests to investigate the fatigue performance at the welded joint

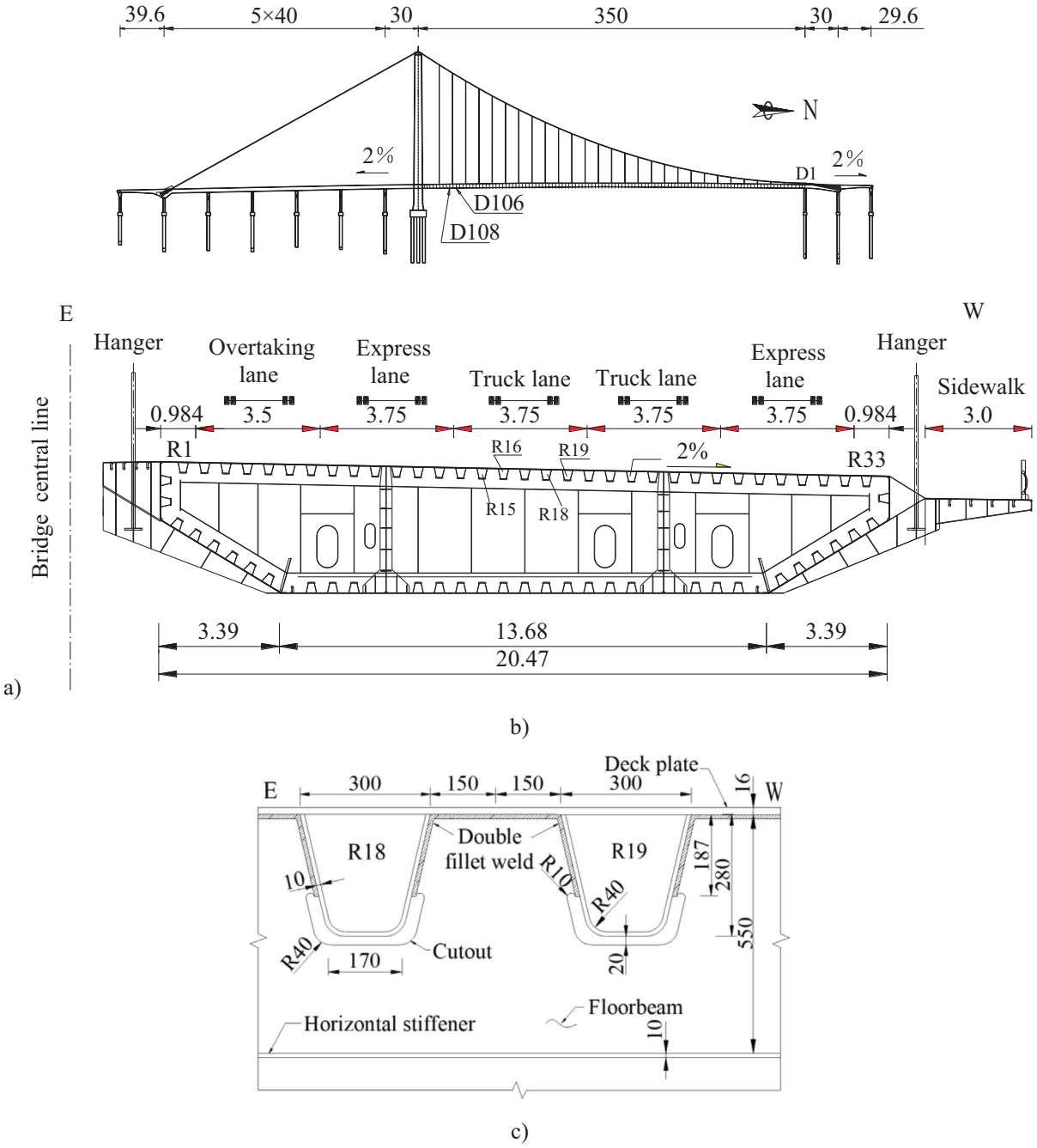

Fig. 2. Pingsheng Bridge, a) elevation layout (Unit: m); b) cross section of steel box girder (Unit: m); c) OSD (Unit: mm).

between a thickened-edge U-rib and the deck plate in the OSDs. They estimated the HHS at this detail based on the stress measured at 5 mm and 15 mm location from the weld toe, and found that the rolled U-ribs with thickened edges may reduce the probability of fatigue cracking at the weld toe of ribs, while it may not aid in fatigue resistance at the weld root. Wu [21] also studied the fatigue crack of the RD detail using linear-elastic fracture mechanics and the HSS method, and they added a geometric correction factor to the empirical equations to improve the estimation of crack propagation life.

Wang [22] investigated the fatigue resistance of two types of RF weld using the HSS method. The tests concluded that the detail with a vertical transition configuration showed a higher fatigue strength than that of the circular arc transition at cope holes on the floorbeams. Yokozeki [23] investigated the connection detail between longitudinal ribs and floorbeams using the HSS method. The test results indicated that the connection with a silt crossbeam lowered the fatigue performance at this detail. Huang [24] performed full-scale fatigue tests to investigate the crack propagation characteristics at the weld toe at the lower end of RF weld. The results indicated that the HSS in combination with FAT90 can be used to evaluate the fatigue performance at this detail. Experimental tests and FEM analyses performed by Cheng [25] investigated the effect of employing UHPC overlay on the HSS at fatigue-prone details of the OSD. In their study, the cutout geometry employed a large radius at the lower end of RF weld. The results indicated a significant reduction on the HSS at the cutout detail with a 60 mm UHPC overlay. The stress measured by strip strain

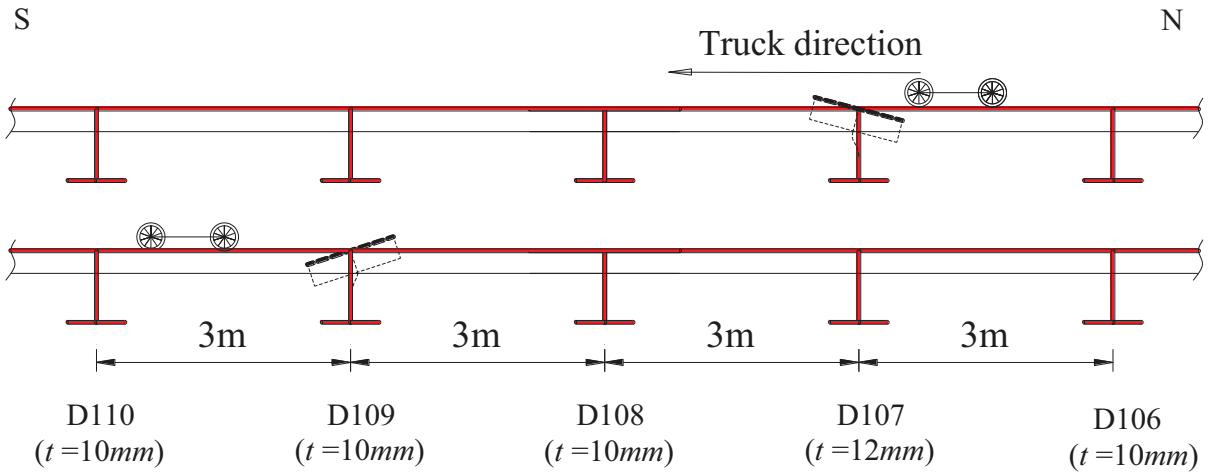

Fig. 3. Diaphragm arrangement with respect to traffic on bridge deck.

gauges showed that for the OSDs without the UHPC overlay, the stress distribution near the cutout detail followed a quadratic manner, and the HSS at the cutout detail can be estimated by the IIW quadratic extrapolation using the stress at location of 0.4 *t*, 0.9 *t* and 1.4 *t*, where *t* is the diaphragm thickness. It was found that for the OSDs with a UHPC overlay, the stress distribution near the cutout detail showed a linear manner. Di [26] recorded the stress at the floorbeam cutout in the OSDs under actual traffic flows. They estimated the HSS at this detail with strain gauges located 5 mm and 15 mm away from the free edge of cutout. The results showed significantly high stresses at the cutout detail, while they did not discuss the stress difference at the two reference points.

Although the HSS method has been applied to fatigue evaluation of the OSD in recent years, most of studies focused on fatigue behavior at the RD or RF details, where the HSS is originally defined at the weld toe. Compared to the stress distribution near the RD or RF details, a significant stress concentration often appears at the floorbeam cutout detail, and it is highly dependent on the cutout geometry [14]. It is not clear if the current code provided HSS model can deal with different cutout geometries due to few available studies on this topic. With above considerations, this study will investigate the application of HSS method to fatigue evaluation of floorbeam cutout detail based on field measurement in the Pingsheng Bridge, where fatigue cracks at cutout detail was observed after only several years of operation.

Characterized by the realistic structural layout, connection details, structural supports and the on-site truck passage representing normal traffic condition, as well as truly welding process and control, the field measurement on bridges is commonly recognized as a reasonable way to investigate stress behaviors of bridge components and their details. However, due to the complicate or even difficult conditions involved in the field test, only few researchers reported their fatigue investigations of the OSD based on the stress measurement at fatigue-prone details [27–29]. Zhu [14] performed simultaneous stress monitoring at cutout detail of two types of closely spaced cutout geometry underneath the same design wheel track. Based on measured nominal stress, they concluded that, compared to the cutout detail with small-radius geometry, the cutout detail with large-radius geometry increased the stress level both at the cutout detail and the detail of rib wall at cutout, and eventually lowered the fatigue life at both the RF detail and the cutout detail.

The present study has been carried out on a floorbeam inside the steel box girder of the Pingsheng Bridge. After applying several groups of strain gauges on the diaphragm web close to the cutout detail, simultaneous stress monitoring was performed under the passage of random traffics. The focus of this study is to investigate

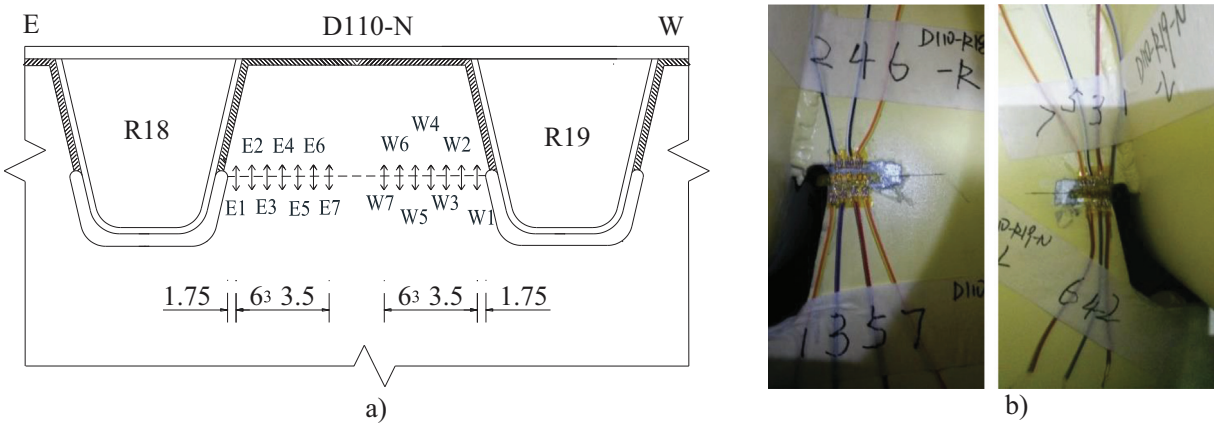

Fig. 4. Strain gauges arrangement, a) location; b) on real bridge.

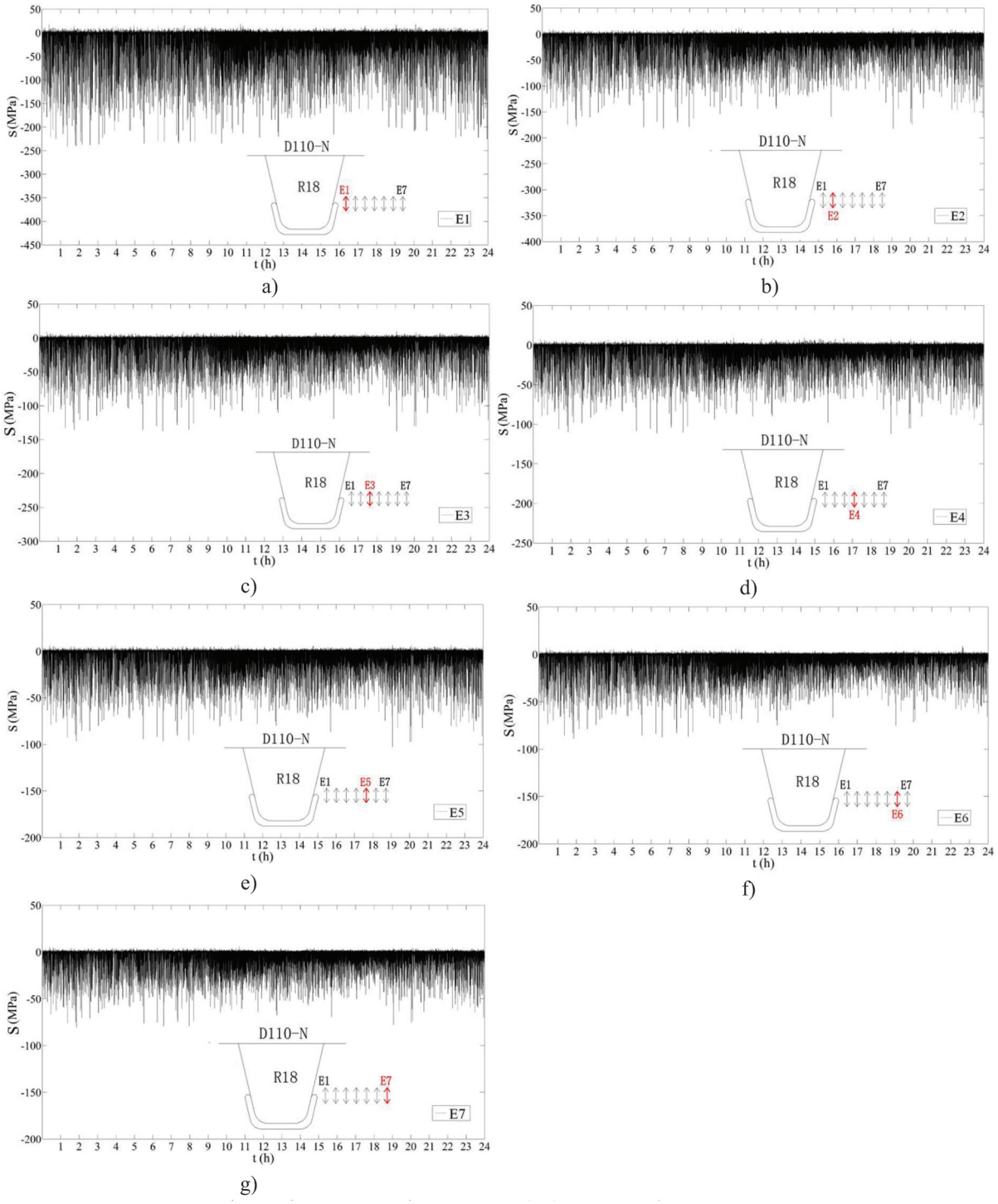

Fig. 5. 24 h stress records at R18-W, a)-g) corresponds to gauge E1 to E7.

currently code-provided HSS models applied to fatigue evaluation of the cutout detail, in which its stress behavior is characterized by severe stress concentration and is highly dependent on the cutout geometry. Then, a HSS model is established based on the stress feature at the area adjacent to the cutout detail. This model is capable of providing a reasonable estimation on the HSS and fatigue life for two different types of cutout geometry with a small or large radius at the cutout detail.

2. Bridge layout and test setup

2.1. Bridge layout

Located in Foshan City, Guangdong Province, mainland China, the Pingsheng Bridge is a self-anchored suspension bridge with only one single tower and a suspended main span of 350 m. Its elevation layout is shown in Fig. 2a). The bridge consists of two pairs of main cable,

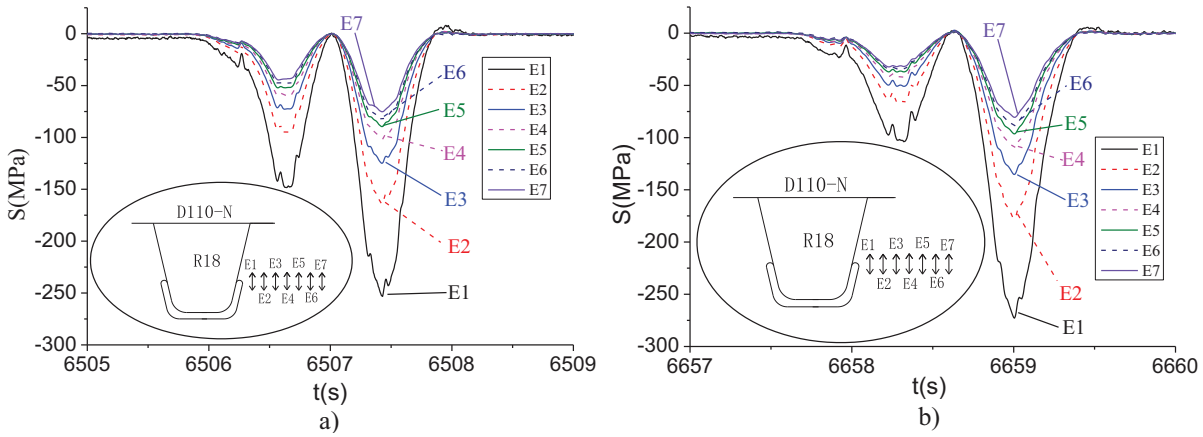

Fig. 6. Stress records produced by two individual truck at R18-W, a) Truck 1; b) Truck 2.

which are supported at the top of main towers and anchored at both ends of the stiffening girder. The stiffening girder is a hybrid one with 10 continuous spans, and it is a steel box girder supported by hangers in the main span and a prestressed concrete box girder supported by concrete piers in the side spans. The south bound and north bound roadways are provided by two separated box girders. In the main span, each steel box girder is 3.5 m high at its central line, and its out-to-out width is 26.1 m. The top flange of the steel girder measures 20.5 m, which provides five one-way traffic lanes on the bridge deck, including the overtaking lane, the express lane, the two truck lanes and the express lane, from left to right as shown in Fig. 2b). The lower ends of the hangers are connected to the stiffening girder through steel anchorage boxes, which are welded to the hanger diaphragms with their spacing of 15 m in the bridge's longitudinal direction.

The typical steel box girder consists of three chambers formed by two inner and two outer longitudinal diaphragms. The former is 16 mm thick and the latter is 32 mm thick, and the distance between the two inner longitudinal diaphragms is 7.8 m. The top flange of the box girder uses the OSDs, which consists of a deck plates, U ribs and floorbeams of 16 mm, 10 mm and 10 mm (12 mm thick at hangers) thick, respectively. As shown in Fig. 2c), the rib is 280 mm high with their center-to-center distance of 600 mm in the bridge's transverse direction. The cutout geometry at the lower end of the RF weld is narrow with a small radius of only 10 mm, and hereafter it is called the "original cutout" in this study. Solid transverse diaphragms (or floorbeams) are placed inside the box girder at spacing of 3 m in the bridge's longitudinal direction. A horizontal stiffener, which is 10 mm thick and 200 mm wide, and locates 550 mm below the deck plate, is connected to the diaphragm web through a groove weld. A 50 mm thick asphalt overlay is applied on the OSDs, and there is a uniform deck gradient of 2% from the side of the central barrier to the side of sidewalk. As part of an urban expressway around the Foshan City, this bridge was built for a 100 year service life, and was opened to traffic at the end of 2006.

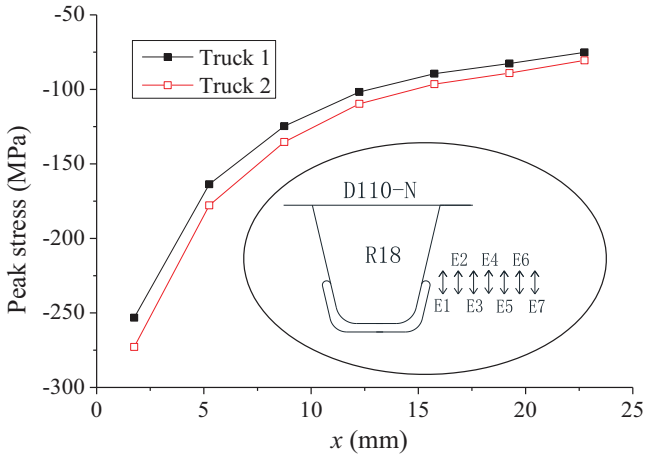

Fig. 7. Peak stress at seven gauges produced by two individual trucks on R18-W.

2.2. Test setup

In this study, the diaphragms inside the steel box girder are numbered from the northern end to southern end of the steel box girder, with the first diaphragm designated as D1, as indicated in Fig. 2a). In addition, each diaphragm has the northern and southern surfaces, which are designated as "N" and "S", respectively. In this way, D110-N represents the northern surface of diaphragm D110. For the longitudinal U ribs, they are numbered from the east side (E) to the west (W) in the bridge's transverse direction, as shown in Fig. 2b). Fig. 3 illustrates five adjacent diaphragms D106-D110 and the traffic direction on the bridge deck, in which D107 is the diaphragm at hangers of 12 mm thickness.

Bridge inspection indicated that more fatigue cracks appeared underneath the design right wheel track in the eastern truck lane shown in Fig. 2, more in detail, at the floorbeam cutout between Rib18 and Rib19 (designated as R18 and R19). In this study, two groups of strain gauge, each group having 7 gauges, were first arranged on the northern surface of the D110 (D110-N), specifically on the western side of R18 (R18-W) and the eastern side of R19 (R19-E). The two groups of strain gauge were symmetric to the central line of the tooth between R18 and R19, with all gauges centered along the critical section (illustrated by dish line), as shown in Fig. 4a). The uniaxial gauges were self-temperature-compensation gauges with gird size of 2.8 mm (length) × 2.0 mm (width). As shown in Fig. 4a), the gauges adjacent to the free edges of cutout were numbered as E1 and W1, respectively, and they centered only 1.75 mm (half width of gauge backing) from the free edge of cutout. Other gauges were closely applied side-by-side. If define x as the distances of gauge to the free edge of cutout, coordinates of the seven gauges will be $x = 1.75, 5.25, 8.75, 12.25, 15.75, 19.25$ and 22.75 mm, respectively. Fig. 4b) shows the installed strain gauges on the real bridge.

The data-acquisition system DH-3820 was mounted inside the box girder and located closely to those gauges. A sampling frequency of 100 Hz was used to measure the dynamic strain response under random traffic flows. In order to obtain strain time histories at different locations, continuous measurement was carried out for one week, including the weekday or weekend. The stress records were obtained

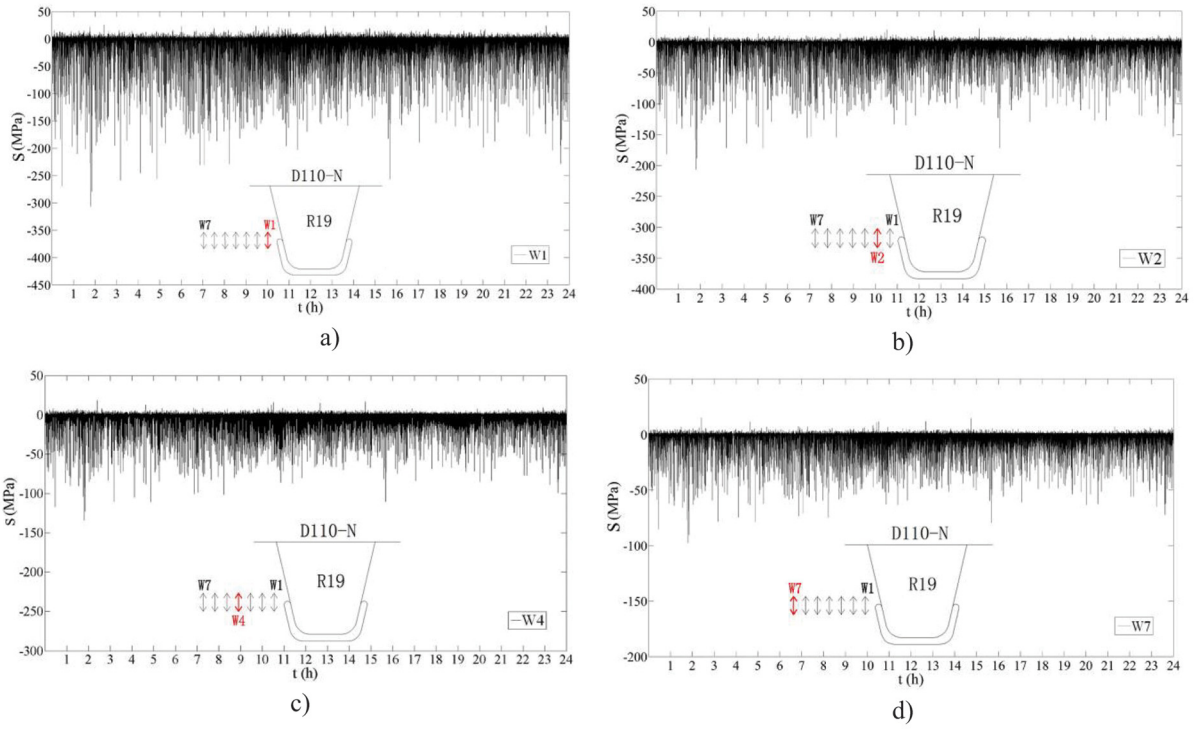

Fig. 8. 24 h stress records at R19-E, a)-d) corresponds to gauge W1 to W7.

using the Young's modulus of 206 GPa of steel (Q345qC) used for the OSD with a yielding strength of 345 MPa and a Poisson's ratio of 0.3.

3. Fatigue evaluation of original cutout detail using HSS models

3.1. Stress time histories

Under passage of random traffic flows, stresses from the strain gauge group on R18-W during continuous 24 h are plotted in Fig. 5. Based on the peak stress tendency, it is clear that the trucks did not evenly pass the bridge during a day, and the stress at cutout detail is always in compression. Comparison among the seven stress time histories from seven different locations indicates that, although their variation shares the same trend, from gauge E1-E7, the stress level is decreased and the decrease is highly dependent on the gauge location. As shown in Fig. 5a), stress level at gauge E1 is the highest, with its maximum peak stress close to 250 MPa. While for gauge E2, although it is directly adjacent to gauge E1, its stress level is sharply decreased, with its maximum peak stress lower than 200 MPa. Meanwhile, stress level at gauge E3 is further decreased compared to that of the gauge E2, and its maximum peak stress is below 150 MPa. The maximum peak stress at gauge E4 is smaller than 110 MPa, with its stress level clearly lower than that of gauge E3. The sharp decrease in stress level from gauge E1-E4 implies that there is a high stress gradient from E1-E4, or there is a severe stress concentration at the free edge of the cutout detail. The significantly high stress and a severe stress concentration suggest that loading effects produced by heavily overweight trucks may contribute to the early crack at the cutout detail. However, from gauge E4-E7, the stress level between adjacent gauges is not so significant compared to that shown in gauge E1-E4. Actually, the stress only shows slight difference between neighboring gauges, as plotted in Fig. 5. This implies that the stress gradient from gauge E4-E7 is significantly reduced.

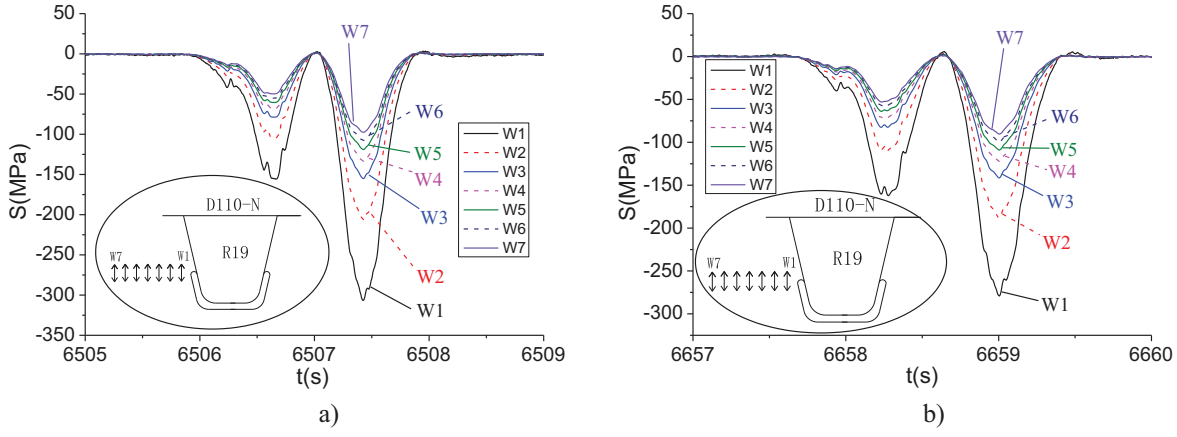

Fig. 9. Stress records from R19-E produced by two individual trucks, a)Truck 1; b) Truck 2.

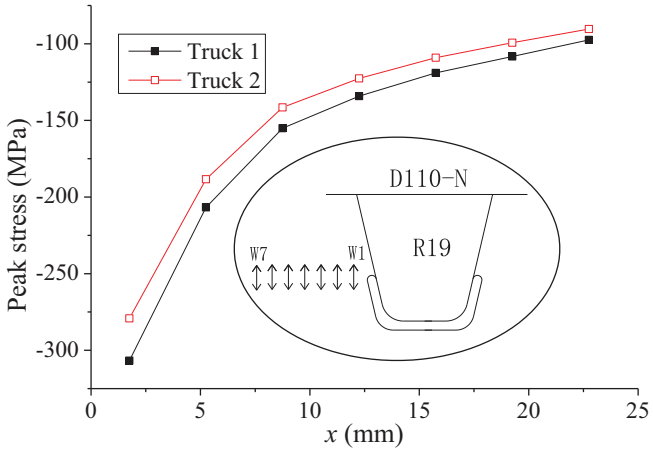

Fig. 10. Peak stress at seven gauges produced by two individual trucks on R19-E.

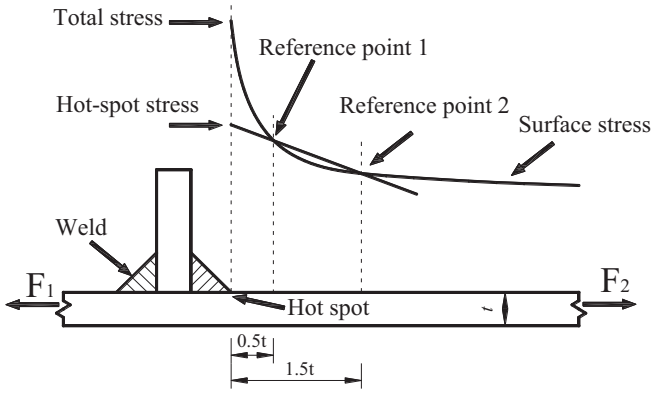

Fig. 11. Definition of HSS on plate surface.

Fig. 6 plots stress records generated by two individual trucks passing the bridge during two different period of time. Although the peak stress at gauge E1 produced by Truck 1 is slightly lower than that of Truck 2, the two trucks generated similar stress curves at all gauges, i.e., two clearly separated stress peaks and significantly high stress produced by their rear axles. The possible reason behind the events causing such significant loadings, is that heavily loaded trucks carrying steel produces (i.e., stainless steel coils) from a steel market in one side of the bridge to many factories on another side of the bridge. Analogously, the peak stresses tend to decrease rapidly from E1-E4 with an increase in their distance to the free edge of cutout, while the peak stresses only show slight decrease with a further increase in their distance to the free edge of cutout, such as E4-E7. This agrees well with the peak stress tendency shown in Fig. 6, and it clearly demonstrates that a significant stress concentration only occurs among a narrow area covered by gauge E1-E4, more in detail, about 10 mm, or 1.0 t to the free edge of cutout, where t is the thickness of the floorbeam web.

In order to clearly show the stress distribution along the critical section, Fig. 7 plots the peak stress from the seven gauges on R18-W, produced by the rear axle of the two trucks during different time. It is clear that the two curves share the same trend. The gauge peak stress tends to increase when it is close to the free edge of cutout. More specifically, the peak stress seems to linearly increase with the decrease in x when $x \geq 1.0$ t, while peak stress shows nonlinear increase when $x <$ 1.0 t.

Meanwhile, stresses from the strain gauge group on the eastern side of R19 (R19-E) during continuous 24 h were also recorded simultaneously and plotted in Fig. 8. Compared to the stress records in Fig. 5, the same traffic flow created slightly high stress level on R19-E, implying that the truck right wheel was close to R19. This may explain why more cracks appeared at the cutout detail on R19-E. In addition, comparison on the stress level among W1-W7 also exhibits a sharp decrease in gauge W1-W4, and a slow decrease in gauge W4-W7, which agrees well with that observed in Fig. 5.

Fig. 9 also shows the stress records produced by the same trucks as that shown in Fig. 6. The two trucks generated slightly higher peak stress in gauge W1 than that of gauge E1, but the stress curves exhibit almost the same feature as that shown in Fig. 6. This means that a severe stress concentration may also occur on R19-E, and the observed more cracks on this side may result from its even high stress produced by passing trucks.

Fig. 10 also plots the peak stresses of the seven gauges on R19-E, which were produced by the rear axle of the two individual trucks. It is clear that the two curves share the same trend. Similar to the stress distribution on R18-W, gauge peak stress increases with the decrease in x, while the peak stress shows more rapid and nonlinear increase when $x \leq 1.0$ t. This again indicates a severe stress concentration occurred close to the free edge of cutout detail.

As indicated above, a nonlinear stress gradient appears at the location close to the free edge of cutout, more in detail, about 1.0 t from the free edge of cutout. Hence the nominal stress among this area may not be well defined at this detail. Although there is a suggested nominal stress location 5 or 6 mm away from the free edge [30], for the original cutout geometry, this location may be still in the stress highly concentrated area. Although the suggested nominal stress method may be applied to a specific type of cutout geometry [12], it is not clear if the method can be used to evaluate fatigue life at cutout detail with different cutout geometry, such as cutouts with different radius at the lower end of RF weld.

3.2. HSS using existing models

For welded connections, the weld toes are the location where stress raiser may present while welding defects are often incorporated, such as weld cracks, porosities, undercuts, slag inclusions and incomplete fusions, etc. Due to rapid heating and cooling in weld process, the residual stress, which is always in tension at weld toe, would also create after welding. As a result, fatigue cracks are frequently observed at weld toe. The hot spot on welded structures, as indicated in Fig. 11, refers to a weld toe on the structural surface where fatigue cracking may occur. The HSS method was initially developed for the fatigue evaluation of tubular- and plate-type- structures with welded steel joints of ships and offshore structures, where there is no clearly defined nominal stress due to complicated connections. Based on its definition, the HSS incorporates all stresses produced at the weld toe, except for the stress contributed by the local weld profile, as shown in Fig. 11. Compared to the nominal stress using a group of S-N curves for different connection details [31], the IIW recommendations define only two FAT categories for HSS approach [15], i.e., the FAT90 for load carrying and the FAT100 for non-load carrying welded details, with their S-N curves defined by

Table 1
Existing HSS models.

Code	Existing HSS models	Reference point location
DNV	(1) $\sigma_{hs} = 1.5\sigma_{0.5t} - 0.5\sigma_{1.5t}$	0.5 t, 1.5 t
	(2) $\sigma_{hs} = 1.875\sigma_{0.5t} - 1.25\sigma_{1.5t} + 0.375\sigma_{2.5t}$	0.5 t, 1.5 t, 2.5 t
	(3) $\sigma_{hs} = 1.12\sigma_{0.5t}$	0.5 t
IIW	(1) $\sigma_{hs} = 1.67\sigma_{0.4t} - 0.67\sigma_{1.0t}$	0.4 t, 1.0 t
	(2) $\sigma_{hs} = 2.52\sigma_{0.4t} - 2.24\sigma_{0.9t} + 0.72\sigma_{1.4t}$	0.4 t, 0.9 t, 1.4 t

their fatigue strength at 2 million cycles. The only two design categories clearly simplify the fatigue evaluation for steel structures.

Determination of the HSS is based on the stress at two or three reference points in a specific distance to the weld toe, which is normalized by plate thickness as to account for plate thickness effects. The main concern for reference points is that stress nonlinearity due to notch singularity at weld toe will be excluded. The well-known extrapolation models for the HSS suggested by DNV [31] and IIW [15] are shown in Table 1. Based on the number of reference points, the two-point model provides a linear calculation of the HSS, while the three-point model yields a quadratic estimation of the HSS at the weld toe.

In Table 1, σ_{hs}denotes the HSS at the weld toe; $\sigma_{\alpha t}$ is the surface stress at the reference points located αt away from the hot spot, in which α is a distance factor and can be the value of 0.4, 0.5, 0.9, 1.0, 1.5 and 2.5, respectively.

Because Truck 2 produced higher stress response on R18-W, while Truck 1 generated higher stress response on R19-E, those high peak stresses, as shown in Figs. 7 and 10, will be used to calculate the peak HSS at the free edge of cutout based on the existing HSS models listed in Table 1. The fitted peak HSS from gauges on R18-W and R19-E are plotted in Fig. 12. It shows a sharp increase in stress at the free edge of cutout, and the stress distribution along the critical section is characterized by significant nonlinearity. Because the estimated HSS is higher than the yielding stress of the steel, such high stress may not be the reality and hence should not be considered in the present study.

Fig. 12 also presents the peak HSS at the free edge of cutout estimated by the five existing HSS models. The DNV(3) predicts the lowest peak HSS, while the IIW(1) provides the highest estimation. Other models predict intermediate results, and the peak HSS from the DNV (1) almost equals to that of IIW(2). Because the highest peak HSS is over 50 MPa higher than the lowest one, based on relationship between fatigue life and cubic stress range per AASHTO LRFD [32], the calculated fatigue life may differ quite a lot if the existing HSS models are used.

3.3. Fatigue life estimation using existing HSS models

Based on simultaneous measurement at each gauge group, the HSS time histories at the free edge of cutout can be calculated using the five existing HSS models through extrapolation. Then, the rainflow counting method [33] is employed to process the stress time histories, as to obtain the stress-range histograms at the two locations. With Miner's rule on cumulative fatigue damage [34], the effective stress ranges S_{reff} can be calculated as Eq. (1) [35].

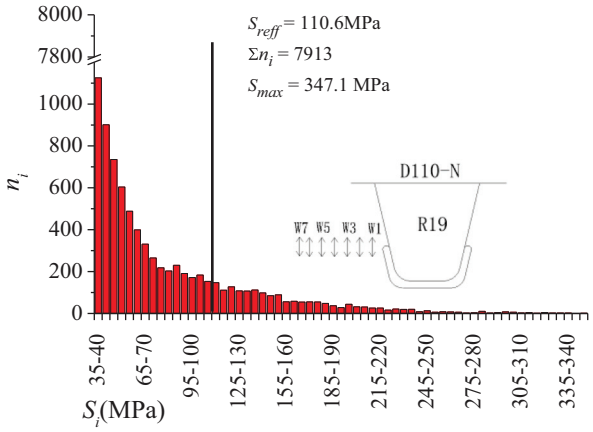

Fig. 13. Estimated HSS spectrum based on linear extrapolation from gauges W1 and W2.

$$S_{reff} = \left[\sum\left(n_i s_i^3 / \sum n_i\right)\right]^{1/3} \quad (1)$$

where n_i and $\sum n_i$denotes the number of loading cycles under stress range of S_i and the total number of effective loading cycles. Because fatigue contribution from much low stress ranges can be negligible, for the variable-amplitude fatigue loading, the cutoff stress ranges of the FAT90 and FAT100 are applied, and the stress ranges lower than 35 MPa are discarded, as shown in Fig. 13.

Fig. 13 plots the estimated HSS stress-range spectrum at free edge of cutout detail on R19-E, which is obtained by linear extrapolation of stress measured at W1 and W2 during 24 h. It is found that the calculated maximum stress range is as high as 347.1 MPa, indicating that the free edge of cutout experienced significantly high stress. As regards stress ranges higher than 250 MPa, their loading cycles are small during one day. Calculation based on Eq. (1) provides the effective stress ranges and the number of loading cycles of 110.6 MPa and 7913, respectively. Meanwhile, the estimated fatigue life at the free edge of cutout will only be 0.37 years for FAT90 and 0.51 years for FAT100 (see Table 2), which is significant lower than the observed fatigue life on the real bridge. It is noted that stresses at gauges W1 and W2 typically include nonlinear stress compared to other gauges on the western side of W2, as shown in Fig. 7. Consequently, if the nonlinear peak stress does not exclude in the HSS, the obtained fatigue life may be significant low due to the significantly overestimated HSS.

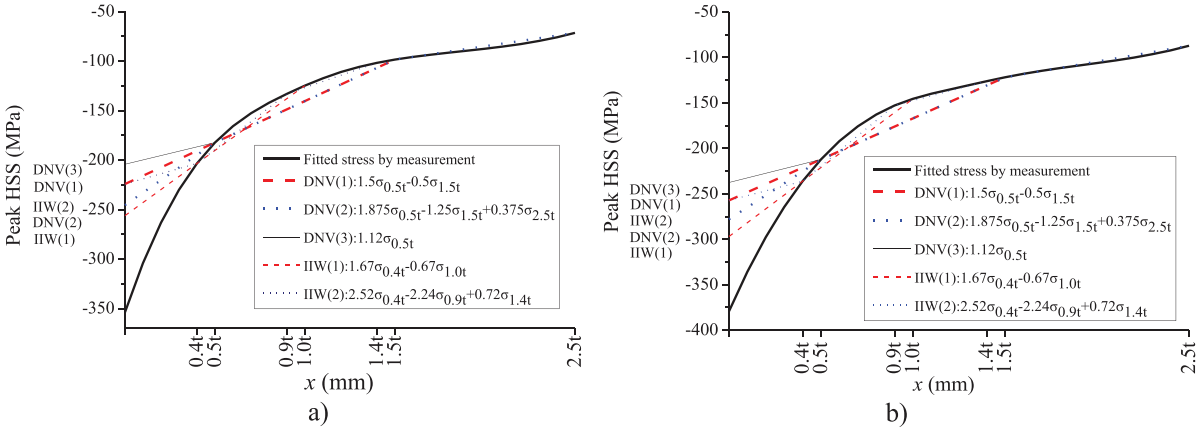

Fig. 12. Peak HSS, a) on R18-W; b) on R19-E.

Table 2
Estimated fatigue life based on various HSS models.

HSS models	S_{reff}	$\sum n_i$	Y	
			FAT90	FAT100
DNV(1)	83.5	4476	1.53	2.10
DNV(2)	89.0	5333	1.1	1.5
DNV(3)	78.8	4033	2.0	2.8
IIW(1)	90.1	5374	1.0	1.4
IIW(2)	96.8	6330	0.7	0.9
Linear extrapolation	110.6	7913	0.37	0.51
Present model	71.9	3159	3.35	4.52

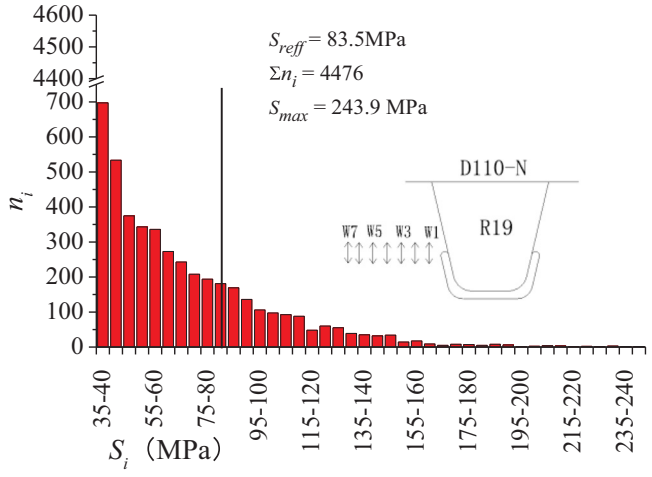

Fig. 14. Estimated HSS spectrum based on DNV(1).

Fig. 14 shows the stress-range spectrum, the effective stress range and number of loading cycles at the free edge of cutout, using the DNV (1) listed in Table 1, in which the stress reference points respectively locate at 0.5 t and 1.0 t from the free edge of cutout. The calculated effective stress range is 83.5 MPa, which is significantly lower than that extrapolated by W1 and W2 shown in Fig. 13. Meanwhile, the number of loading cycles is also notably decreased. Using the FAT90 and FAT100, the estimated fatigue life at the cutout detail increases to 1.53 and 2.10 years, respectively. However, the estimated fatigue life is still substantially lower than the observed fatigue life on the real bridge. Although the stress at the second reference point (1.0 *t*) does not clearly show stress nonlinearity, the nonlinear stress at the first reference point (0.4 *t*) can be clearly identified. Hence the calculated HSS at the free edge of cutout may still include nonlinear stress, and the HSS may still be overestimated, resulting in a significantly shorter fatigue life than the observed one on the real bridge.

Table 2 lists the calculated effective stress ranges and loading cycles based on other HSS models, i.e., DNV(2) and DNV(3), as well as IIW (1) and IIW(2), while their estimated fatigue life per FAT90 and FAT100 are also provided. Because the first reference point of the four models locates on the western side of gauge W2, and their distances to the free edge of cutout is shorter than 1.0 t, the nonlinear stress is not excluded in the measured stress. Consequently, the calculated HSS at the free edge of cutout may also be high, and their estimated fatigue life is significantly lower compared to the observed fatigue life on the real bridge.

3.4. Suggested HSS models at cutout detail

As foregoing reasons, if the stress reference points locate too close to the free edge of the cutout detail, due to the effect of nonlinear stress, the calculated HSS at the free edge of cutout may be significantly overestimated, resulting in a substantially underestimated fatigue life. Considering the measured stress at gauge E3 and its western side gauges (shown in Fig. 5), as well as gauge W3 and its eastern side gauges (shown in Fig. 8), their stress behave in a linear way, indicating that the stress in the area beyond E3 or W3 is not affected by the nonlinear stress emanating from significant stress concentration at the free edge of cutout.

Following the concept of HSS method, this study presents a novel HSS model with its stress reference points respectively located 1.0 t and 1.5 t away from the free edge of cutout, which can be expressed as,

$$\sigma_{hs} = 3.0\sigma_{1.0t} - 2.0\sigma_{1.5t} \tag{2}$$

Compared to the existing HSS model shown in Table.1, the present HSS model simply uses a linear extrapolation to estimate HSS stress at the cutout detail, but the two reference points locate far from the free edge of cutout. As a result, nonlinear peak stress can be excluded at two reference points.

Fig. 15 plots the stress-range spectrum, the effective stress range and number of loading cycles at the free edge of cutout based on the present HSS model. The calculated effective stress range is 71.9 MPa, which is 13.7% lower than that determined by DNV(1), and the number of loading cycles decrease to 3159. Using the FAT90 and FAT100, the estimated fatigue life at the cutout detail increases to 3.35 and 4.52 years, respectively. Because the fatigue life of 4.52 years is close to the observed fatigue life on the real bridge (about five years), the present HSS model in combination with the FAT100, may provide an acceptable estimation on fatigue life at original cutout detail.

4. Fatigue evaluation of retrofit cutout geometry using various HSS models

As regards the early fatigue cracking at free edge of cutout detail shown in Fig. 1, a retrofit plan using a new cutout geometry (designated as the retrofit cutout geometry) was put forward and tentatively applied around R15 and R16 on D106 of the Pingsheng Bridge in 2015, because the bridge authority was not sure if the new cutout geometry was good for bridge retrofit to prevent fatigue cracking at the cutout detail. The retrofit cutout, as shown in Fig. 16, was formed on the original cutout by cutting off more floorbeam web material close to the ribs. Compared to the original cutout geometry shown in Fig. 2, the retrofit cutout geometry employed an increased radius of 35 mm at the lower end of RF weld, hence the cutout is enlarged. Such kind of retrofit may help reduce out-of-plane distortion at the cutout detail, but may

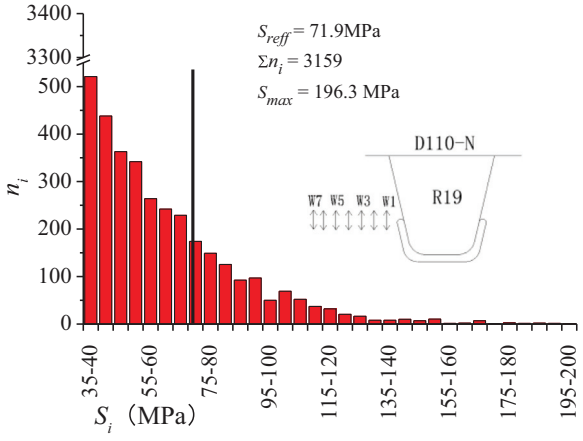

Fig. 15. HSS spectrum and effective stress range calculated by suggested model.

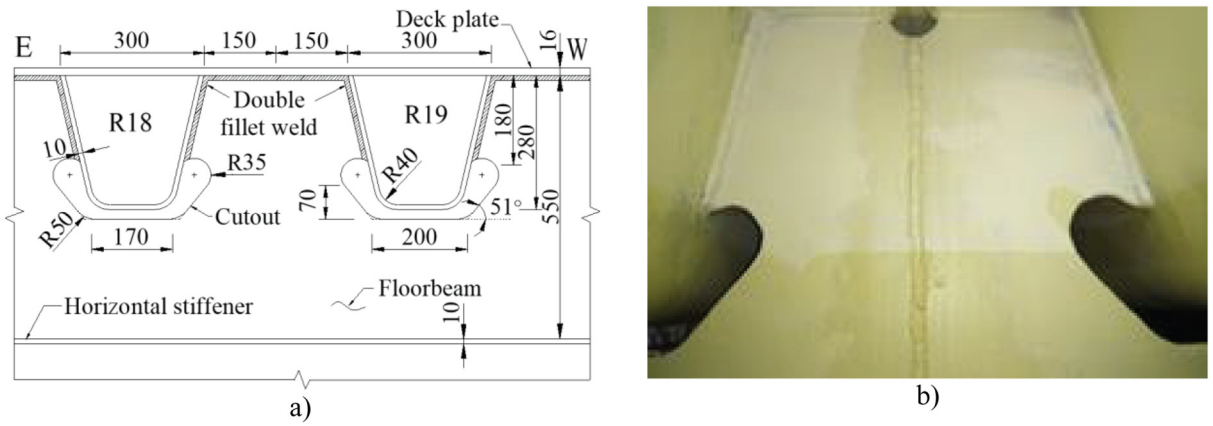

Fig. 16. Retrofit cutout geometry, a) structural layout; b) on real bridge.

weaken the floorbeam web and increase in-plane stress under wheel loads [14].

Two groups of gauges, each having seven gauges, were also respectively applied on the northern surface of D106, with e1-e7 applied on the western side of R15 (R15-W) and w1-w7 applied on the eastern side of R16 (R16-E), as shown in Fig. 17. It is noted that the applied gauge area between R15 and R16 was directly underneath the designed left wheel track, and was within the same traffic lane shown in Fig. 2. Statistically, the tentative retrofit cutout detail could experience the same traffic loads as the tested original cutout detail. In addition, all gauges centered along the critical section, with their distance to the free edge of cutout measured 1.75, 5.25, 8.75, 12.25, 15.75, 19.25 and 22.75 mm, respectively.

The recorded stress time histories at strain gauge group on R15-W of D106 during continuous 24 h are plotted in Fig. 18. It is clear that stresses from the seven gauges are all in compression, which is in agreement with stress obtained on the original cutout. For the seven gauges, the highest stress response appears at gauge e1, and the stress level first decreases rapidly and then decreases slowly with the increase in distance to the free edge of cutout, which also shows the same trend as the original cutout. Compared to large stress difference between E1 and E2 of the original cutout, stress difference between e1 and e2 is small, indicating that the stress gradient, or the stress concentration close to the free edge of the retrofit cutout detail is decreased.

Fig. 19 plots stress produced by two individual trucks passing the bridge deck during two different period of time. The two trucks generated similar stress curves at the two gauge groups. The maximum peak stress, which was generated at gauge e1, is slightly lower than that shown in Figs. 6 and 9, but the peak stress from gauge e7 is significantly higher than E7 on the original cutout. Consequently, the peak stress from gauges e1-e7 does not show so rapid decrease as observed from E1-E7 of the original cutout, indicating a reduced stress concentration along the critical section.

Fig. 20 plots the maximum peak stress at the seven gauges shown in Fig. 17. It is clear that the two curves share the same trend, and their stresses decrease almost linearly with the increase in their distance to the free edge of cutout, particularly at gauge e3 and its western side gauges. Compared to Fig. 7, although the peak stress at gauge e1 is lower than gauge E1, the peak stresses at gauges e2-e7 are higher than gauges E2-E7, hence stress distribution along the critical section shows difference. Based on the above observation, it is clear that the retrofit cutout geometry only reduced the stress at an area directly adjacent to the free edge of cutout, such as the area within 0.5 t to the free edge of the cutout. Beyond this area, the stress does not decrease rapidly. Using the stress curves produced by Truck 1 in Fig. 7 and Truck2 in Fig. 20, Fig. 21 shows the stress ratio along critical section from the two types of cutout geometry, in which the stress ratio of all gauges is the normalized peak stress using the peak stress at gauge E1 or e1. Compare to the original cutout, although the retrofit cutout geometry significantly reduced stress gradient along the critical section, it may increase the stress level at the area beyond 0.5 t from the free edge of cutout. If nominal stress 6 mm away from the free edge of cutout is employed for cutout detail, the fatigue stress may increase at the retrofit cutout geometry. As a result, the evaluated fatigue life may be significantly low. Such structural rehabilitation plan using the retrofit cutout geometry would not improve the fatigue performance at the cutout detail based on the nominal stress method [14].

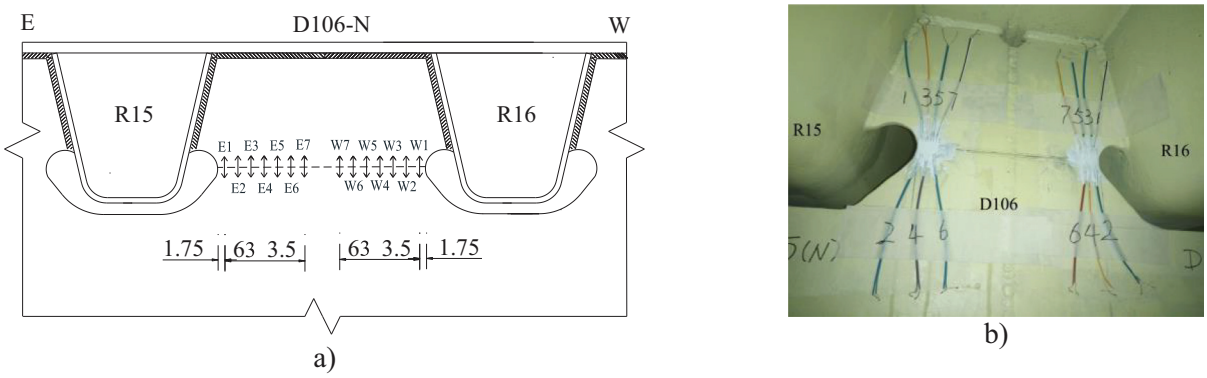

Fig. 17. Strain gauges close to retrofit cutout detail, a) arrangement; b) on real bridge.

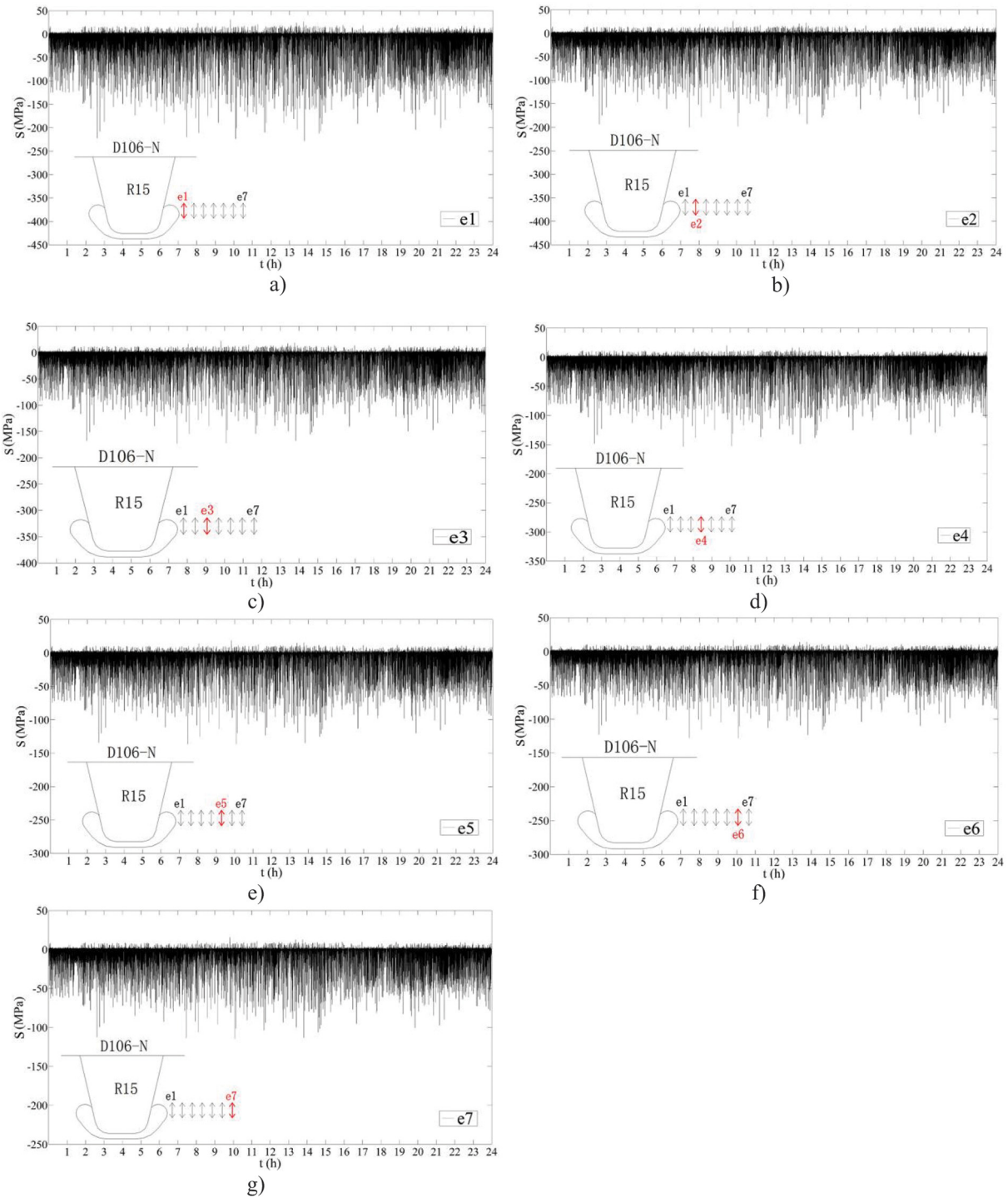

Fig. 18. 24 h stress records at R15-E, a)–g) corresponds to gauges e1 to e7.

Based on the measured peak stress along the critical section, Fig. 22 plots the calculated HSS at the free edge of cutout using the existing HSS models and the present model. Compared to Fig. 12, the existing models and the present model provide linear estimation of HSS, regardless the location of reference points. This is because the retrofit cutout geometry greatly reduces the stress concentration at the free edge of cutout, and the sharp increase in stress at the free edge of the original cutout characterized by nonlinear effect is clearly disappeared. As regards the present HSS model, its estimated HSS agrees well with various models, although its first reference point to the free edge of cutout is relatively far compared to that in the existing HSS models.

With simultaneous stress records at each gauge group, stress time histories at reference points can be obtained through interpolation. Then the HSS time histories at the free edge of cutout can be determined using various HSS models. The HSS level at R15-W is slightly higher than that at R16-E, and fatigue life estimation also indicates a lower life at R15-W. Hence, stress from R15-W will be presented in the following.

Fig. 23 illustrates the stress-range spectrum, the effective stress range and number of loading cycles using the DNV(1) model and the

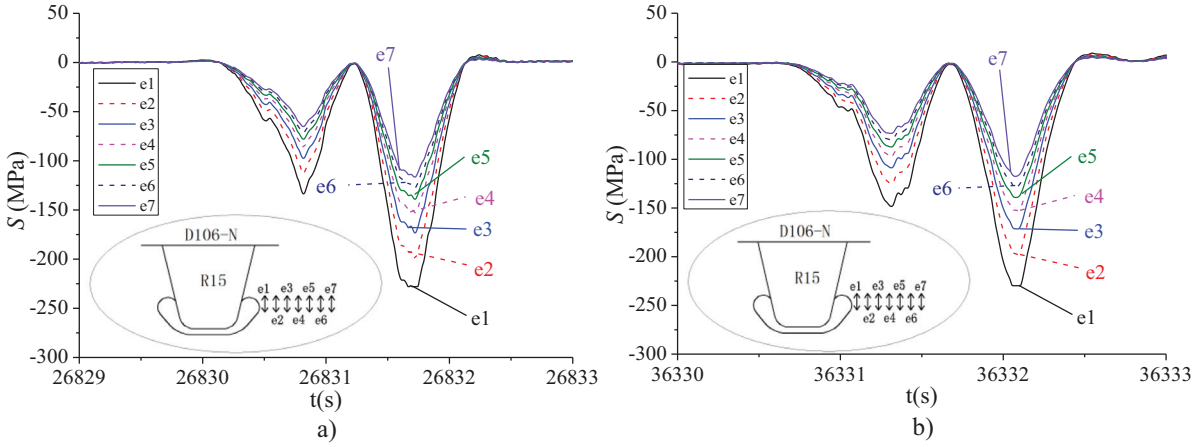

Fig. 19. Stress records produced by two individual trucks on R15-W, a) Truck 1; b) Truck 2.

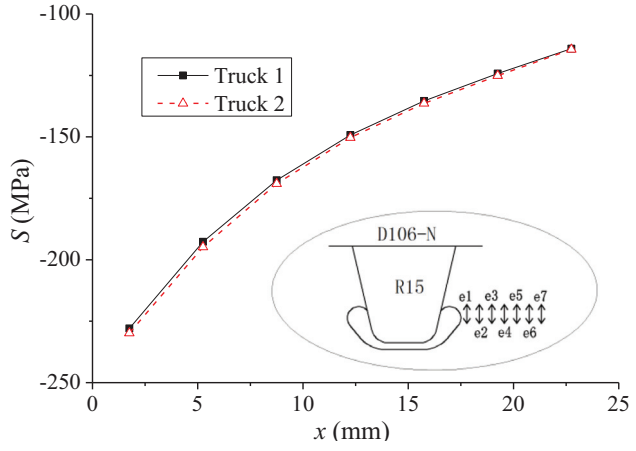

Fig. 20. Peak stress along critical section produced by two individual trucks.

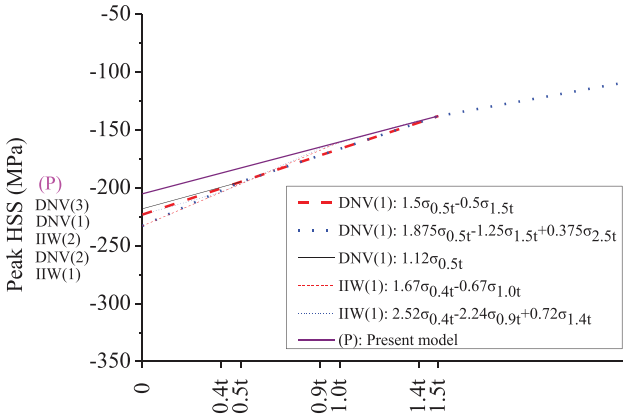

Fig. 22. Peak HSS on R15-W from various HSS models.

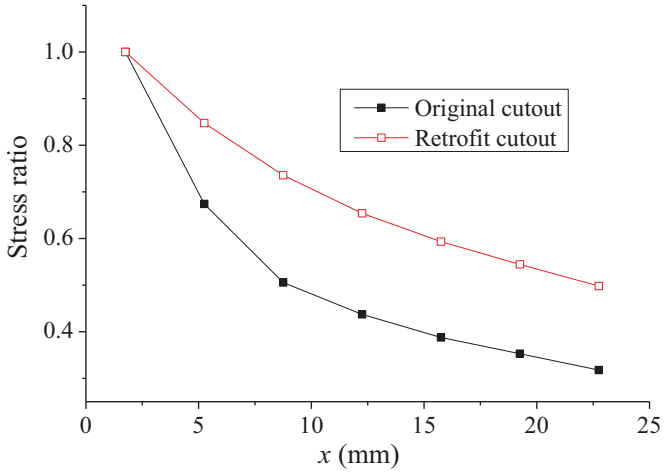

Fig. 21. Stress ratio along critical section of floorbeam considering two types of cutout geometry.

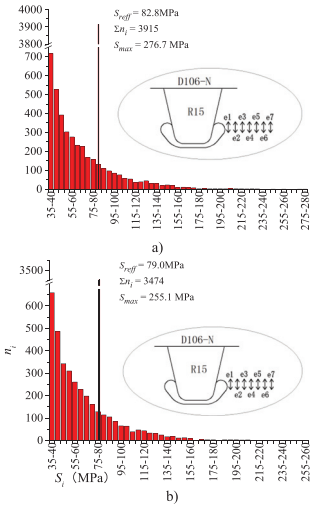

Fig. 23. HSS spectrum estimated at R15-W, a) by DNV(1); b)by present model.

present HSS model. The effective stress range and loading cycles is 82.8 MPa and 3915 based on DNV(1), which is slightly lower than that estimated at R18-W in Fig. 14. Using the FAT100, the estimated fatigue life at the cutout detail is 2.5 years, as shown in Table 3. As regards the present HSS model, the effective stress range and number of loading cycles are respectively 79.0 MPa and 3474, which is higher than that of the original cutout. The possible reason is that although the measured stress

Table 3
Estimated fatigue life based on HSS at R15-W.

HSS models	S_{reff}	$\sum n_i$	Y (FAT100)
DNV(1)	82.8	3915	2.5
DNV(2)	84.6	4176	2.2
DNV(3)	81.9	3755	2.7
IIW(1)	84.7	4216	2.1
IIW(2)	86.9	4543	1.8
Present model	79.0	3474	3.2

level at gauge e1 is slightly lower than the stress level at gauge W1, the stress level from gauges e2-e7 are higher than gauges W2-W7 due to rapid decrease in stress on R19-E. Because the present HSS model uses the reference points located beyond gauge e2, the estimated HSS level at the retrofit cutout detail will be certainly higher than that at the original cutout. Table 3 lists the estimated fatigue life at R15-W using the HSS models, including the present model. It is clear that the estimated fatigue life are close to each other, suggesting that the present HSS model can also be applied to cutout detail with a large radius at the lower end of RF weld.

Using the present HSS model with FAT100, the estimated fatigue life at the retrofit cutout detail is only 3.2 years. It is significantly shorter than the remaining life of the bridge, and it is also shorter than the fatigue life of the original cutout detail. Hence the retrofit cutout geometry will not improve fatigue performance of the cutout detail on the real bridge.

5. Conclusions and remarks

Based on simultaneous stress measurement along the critical section of floorbeam cutout under random traffic flow, applicability of the existing HSS models to cutout detail is investigated for the original cutout geometry. Then a new HSS model is presented and validated for both the original cutout and the retrofit cutout geometry. The following conclusions and remarks can be made.

1) Close to the free edge of cutout, the original cutout geometry presented significantly nonlinear stress and a high stress gradient along the critical section due to its smaller radius at cutout, while the retrofit cutout geometry with a larger radius almost eliminated significantly nonlinear stress and hence reduced the stress gradient. Meanwhile, the retrofit cutout geometry decreased the stress at the area adjacent to free edge of cutout detail, but it increased the stress beyond 0.5 t along the critical section.
2) For the original cutout detail, the existing HSS models estimated significantly shorter fatigue life than that observed on the real bridge due to their first reference points located too close to the free edge of cutout. Because the nonlinear stress is not excluded in the models, overestimated HSS at the cutout detail would occur.
3) A new HSS model was presented with its two reference points located respectively 1.0 t and 1.5 t away from the free edge of cutout. The model can exclude nonlinear stress in the estimated HSS, and the evaluated fatigue life at the original cutout detail using FAT100 agrees well with the observed life on the real bridge. The estimated fatigue life at the retrofit cutout detail also agrees well with the existing HSS models. Hence, the presnt HSS model and FAT100 may be applicable to fatigue evaluation of floorbeam cutout detail with different cutout geometry.
4) Under random traffic flows, a high-level of effective stress range and huge amount of loading cycles are generated at the retrofit cutout detail within test period, and the estimated fatigue life using the various HSS models is less than 3.2 years. Hence the retrofit cutout geometry cannot improve fatigue performance of the cutout detail, and it will not be suggested to retrofit the cutout cracking on the Pingsheng Bridge.

Author statement

All persons who have made substantial contributions to the work are listed in the paper, including those who are not authors are named in the Acknowledgments section. Zhiwen Zhu have made substantial contributions to the conception of this work, drafted the paper and revised it critically for important intellectual content; Jianpeng Li and Yan Huang participated in the field test of this study, and they both performed the statistical analysis. Alberto Carpinteri provided editing and writing assistance. All authors have read and approved the final version to be submitted.

Declaration of Competing Interest

The authors declare that they have no known competing financial interests or personal relationships that could have appeared to influence the work reported in this paper.

Acknowledgements

This work was supported by the National Natural Science Foundation of China (grant number 51878269); the STU Scientific Research Foundation for Talents of China (grant number NTF18014); and the Teaching Team Development Program of Guangdong Higher Education Institutes of China, to which the writers gratefully appreciate.

References

[1] Federal Highway Administration (FHWA), US Department of Transportation Manual for Design, Construction, and Maintenance of Orthotropic Steel Deck Bridges, FHWA, Washington, D.C., 2012
[2] R.C. Battista, M.S. Pfeil, E.M.L. Carvalho, Fatigue life estimates for a slender orthotropic steel deck, J. Constr. Steel Res. 64 (1) (2008) 134–143.
[3] R. Wolchuk, Lessons from weld cracks in orthotropic decks on three European bridges, J. Struct. Eng. 116 (1) (1992) 75–84.
[4] J.H. Cao, X.D. Shao, Z. Zhang, H. Zhao, Retrofit of an orthotropic steel deck with compact reinforced reactive powder concrete, Struct. Infrastruct. Eng. 12 (3) (2016) 411–429.
[5] Z.W. Zhu, Y. Huang, Z. Xiang, Fatigue performance of floorbeam cutout detail of orthotropic steel bridge on heavy freight transportation highway, China J. Highw. Transp 30 (3) (2017) 104–112 (In Chinese).
[6] R.J. Connor, Influence of cutout geometry on stresses at welded RF welds in steel orthotropic bridge decks, J. Transp. Res. Board 1892 (1) (2004) 78–87.
[7] W.D. Corte, Parametric study of floorbeam cutouts for orthotropic bridge decks to determine shape factors, Bridge Struct. 5 (2–3) (2009) 75–85.
[8] Q. Ye, Insights on Analysis and Design of Steel Orthotropic Decks, ASCE/the 4th Orthotropic Bridge Conference Proceedings, September 21–24 2015 35–45 Tianjin, China.
[9] Z.W. Zhu, Z. Xiang, J.P. Li, Fatigue damage investigation on diaphragm cutout detail on orthotropic bridge deck based on field measurement and FEM, Thin Wall. Struct. 157 (2020) 107106.
[10] Z.W. Zhu, T. Yuan, Z. Xiang, Y. Huang, Y. Zhou, X.D. Shao, Stress behaviors and fatigue performance of details in orthotropic steel bridges with UHPC-deck plate composite system under in-service traffic flows, J. Bridg. Eng. 23 (3) (2018), 04017142, .
[11] L. Deng, S.Q. Zou, W. Wang, X. Kong, Fatigue performance evaluation for composite OSD using UHPC under dynamic vehicle loading, Eng. Struct. 232 (2021) 111831.
[12] BS5400-10C-1980 Steel, Concrete and Composite Bridges: Part 10: Charts for Classification of Details for Fatigue, Standards Institution, British, 1999 49–53.
[13] M.S. Pfeil, R.C. Battista, A.J.R. Mergulhao, Stress concentration in steel bridge orthotropic decks, J. Constr. Steel Res. 61 (2005) 1172–1184.
[14] Z.W. Zhu, Z. Xiang, J.P. Li, Y. Huang, S.P. Ruan, Fatigue behavior of orthotropic bridge decks with two types of cutout geometry based on field monitoring and FEM analysis, Eng. Struct. 209 (2020) 109926.
[15] International Institute of Welding (IIW), Recommendations for Fatigue Design of Welded Joints and Components, 2007.
[16] B. Cheng, X.H. Ye, X.G. Cao, D.D. Mbako, Y.S. Cao, Experimental study on fatigue failure of rib-to-deck welded connections in orthotropic steel bridge decks, Int. J. Fatigue 103 (2017) 157–167.
[17] J. Heng, K. Zheng, C. Gou, Y. Zhang, Y. Bao, Fatigue performance of rib-to-deck joints in orthotropic steel decks with thickened edge U-ribs, J. Bridg. Eng. 22 (9) (2017), 04017059, .
[18] Z.Q. Fu, B.H. Ji, C.Y. Zhang, Q.D. Wang, Fatigue performance of roof and U-rib weld of orthotropic steel bridge deck with different penetration rates, J. Bridg. Eng. 22 (6) (2017), 04017016, .
[19] M. Johan, B. Eric, R. Pijpers, Fatigue resistance of the deck plate in steel orthotropic deck structures, Eng. Fract. Mech. 201 (2018) 214–228.

[20] P. Luo, Q. Zhang, Y. Bao, Y. Bu, Fatigue performance of welded joint between thickened-edge U-rib and deck in orthotropic steel deck, Eng. Struct. 181 (2019) 699–710.
[21] W.J. Wu, H. Kolstein, M. Veljkovic, Fatigue resistance of rib-to-deck welded joint in OSDs, analyzed by fracture mechanics, J. Constr. Steel Res. 162 (2019) 105700.
[22] B.H. Wang, P.M. Lu, Y.H. Shao, Research on rib-to-diaphragm welded connection by means of hot spot stress approach, Steel Compos. Struct. 18 (1) (2015) 135–148.
[23] K. Yokozeki, C. Miki, Fatigue evaluation for longitudinal-to-transverse rib connection of orthotropic steel deck by using structural hot spot stress, Weld World 60 (1) (2016) 83–92.
[24] Y. Huang, Q.H. Zhang, Y. Bao, Y.Z. Bu, Fatigue assessment of longitudinal rib-to-crossbeam welded joints in orthotropic steel bridge decks, J. Constr. Steel Res. 159 (2019) 53–66.
[25] B. Cheng, H. Abdelbaset, L. Tian, H.T. Li, Q.T. Su, Hot spot stress investigation on rib-to-deck-to-floor beam connections in UHPC reinforced OSDs, J. Constr. Steel Res. 179 (2021) 106517.
[26] J. Di, X.Z. Ruan, X.H. Zhou, J. Wang, X. Peng, Fatigue assessment of orthotropic steel bridge decks based on strain monitoring data, Eng. Struct. 228 (2021) 111437.
[27] R.J. Connor, J.W. Fisher, Results of Field Measurements on the Williamsburg Bridge Orthotropic Deck-final Report, ATLSS Report No. 01-01, Department of Civil and Environmental Engineering, Lehigh University, Bethlehem PA, January, 2001.
[28] R.J. Connor, J.W. Fisher, Results of Field Measurements Made on the Prototype Orthotropic Deck on the Bronx-Whitestone Bridge-final Report, ATLSS Report No. 04-03, Center for Advanced Technology for Large Structural Systems, Lehigh University, Bethlehem PA, 2004.
[29] R.J. Connor, J.W. Fisher, Field testing of orthotropic bridge decks, Steel Struct. 5 (2005) 225–231.
[30] R.J. Connor, J.W. Fisher, Consistent approach to calculating stresses for fatigue design of welded rib-to-web connections in steel orthotropic bridge decks, J. Bridg. Eng. 11 (5) (2006) 517–525.
[31] DNV, Recommended Practice DNV-RP-C203, Fatigue Design of Off shore Steel Structure, Det Norske Veritas, Norway, 2006.
[32] AASHTO, AASHTO LRFD Bridge Design Specification, 6th ed. American Association of State Highway and Transportation Officials, Washington D.C., 2012
[33] S.D. Downing, D.F. Socie, Simple rainflow counting algorithms, Int. J. Fatigue 4 (1) (1982) 31–40 January.
[34] M.A. Miner, Cumulative damage in fatigue, J. Appl. Mech. 12 (3) (1945) 159–164.
[35] F. Moses, C.G. Schilling, K.S. Raju, Fatigue Evaluation Procedures for Steel Bridges, NCHRP Report 299, National Cooperative Highway Research Program, Washington, DC, 1987.